



Enhanced stability and dechlorination activity of pre-synthesis stabilized nanoscale FePd particles

Nataphan Sakulchaicharoen^a, Denis M. O'Carroll^{a,*}, Jose E. Herrera^b

^a Department of Civil and Environmental Engineering, University of Western Ontario, 1151 Richmond St. London, ON, Canada N6A 5B9

^b Department of Chemical and Biochemical Engineering, University of Western Ontario, London, ON, Canada N6A 5B9

ARTICLE INFO

Article history:

Received 27 March 2010

Received in revised form 20 August 2010

Accepted 1 September 2010

Available online 8 September 2010

Keywords:

Iron nanoparticles

Pd

Stability

TCE

Dechlorination

ABSTRACT

Nanoscale zero-valent iron (NZVI) particles are promising materials for the in-situ remediation of a wide variety of source zone contaminants. This study presents the results of a systematic investigation of the stability of bimetallic FePd nanoparticle suspensions in water and their capability to degrade trichloroethylene (TCE) synthesized in the presence of various stabilizers (i.e., carboxymethyl cellulose (CMC), polyvinylpyrrolidone (PVP), and guar gum). Results indicate a dramatic improvement in FePd suspension stability when the stabilizer is present in the matrix during the nanoparticle synthesis step. Stability enhancement is controlled by iron nanoparticle/stabilizer electrostatic and steric interactions, which are a function of the molecular structure of the stabilizer. Stabilization mechanisms differed for each stabilizer with CMC and guar gum exhibiting the best nanoparticle suspension stability improvement. Results suggest that the complexation of iron precursors with the stabilizer, during synthesis, plays a key role in nZVI stability improvement. In case of guar gum, gelation during synthesis significantly increased suspension viscosity, enhancing suspension stability. The capability of these materials to degrade TCE was also investigated. Results demonstrated that when stabilizers were present in the matrix dechlorination rates increased significantly. FePd nanoparticles in CMC had the highest observed rate constant; however the highest surface area-normalized rate constant was obtained from FePd stabilized in PVP360K. Results from this study can be used to aid in the selection of appropriate iron nanoparticle stabilizers. Stabilizer selection should be assessed on a case by case basis as no stabilizer will meet the needs of all in-situ remediation applications.

© 2010 Elsevier B.V. All rights reserved.

1. Introduction

The use of zero-valent iron (ZVI) for chlorinated hydrocarbons degradation has been the subject of considerable interest since it was proposed as a remediation alternative in the early 1990s (Matheson and Tratnyek, 1994; Orth and Gillham, 1996; Robert and Stephanie, 1994). This considerable interest is due, in part, to its low cost and low toxicity to the environment in addition to its significant contaminant degradation capabilities (Lien and Zhang, 1999; Liu et al.,

2005). Significant advances have been made related to ZVI for subsurface remediation, including the ability to synthesize nanoscale zero-valent iron (nZVI) (Wang and Zhang, 1997). Originally zero-valent iron particles used for remediation were on the millimetre size range. A decrease in particle size, to the nanometer scale, increases the surface area per gram of ZVI particle by orders of magnitude. Degradation reactions are surface mediated, therefore more surface area results in quicker contaminant degradation (Li et al., 2006; Lien and Zhang, 2001; Wang and Zhang, 1997). nZVI is of particular interest for contaminated site remediation as the particles are theoretically smaller than pores in the soil structure. Given this size it was originally believed that nZVI particles would be able to flow through the pore structure without significant

* Corresponding author. Tel.: +1 519 661-2193; fax: +1 519 661-3942.
E-mail address: docarroll@eng.uwo.ca (D.M. O'Carroll).

mass loss. However unmodified nZVI particles have a strong tendency to aggregate, limiting their subsurface mobility (He and Zhao, 2005; Kanel et al., 2008; Phenrat et al., 2007; Schrick et al., 2004; Zhang and Daniel, 2006).

nZVI agglomeration results from van der Waals and magnetic particle to particle attractive forces (He and Zhao, 2005; Phenrat et al., 2007). To prevent particle aggregation a wide variety of stabilizers have been proposed to modify nZVI particle surface characteristics. Mechanisms that are commonly exploited to improve particle stability in aqueous suspensions include steric and electrostatic hindrance. Steric hindrance occurs when large size stabilizers adsorb on the particle, creating bulky moieties on the particle surface. These moieties prevent interparticle interactions by counteracting particle–particle attractive forces which results in limited particle aggregation. Electrostatic hindrance occurs through an increase in particle net surface charge, leading to repulsive interactions between particles of similar charge (Cosgrove, 2005).

Stabilizers have been used to modify the surface of nZVI particles during (pre-synthesis addition of stabilizer) and following (post-synthesis addition of stabilizer) iron nanoparticle synthesis. Most studies in the literature, however, have investigated the utility of post-synthesis addition. For instance, Saleh et al. (2007, 2008) modified commercially available nZVI (RNIP from Toda Kogyo, Japan) using either a triblock copolymer (PMAA-PMMA-PSS) or a surfactant (SDBS, sodium dodecylbenzene sulfonate). These two post-synthesis modified-RNIP suspensions were more stable than those of bare RNIP. The stability time (time to achieve 50% normalized light intensity) of PMAA₄₈-PMMA₁₇-PSS₆₅₀ and SDBS-stabilized RNIP was around 80 and 25 min, respectively. Whereas the stability time of bare RNIP was only 8 min. In their study, the authors proposed that SDBS improved the colloidal stability via electrostatic interactions, while the triblock copolymer enhanced particle stability via both electrostatic and steric hindrance. In a similar study the ability of post-synthesis addition of anionic polyelectrolytes to stabilize nZVI particles have been evaluated (Kim et al., 2009; Phenrat et al., 2008). The anionic polyelectrolytes evaluated included the sodium salts of polystyrene sulfonate (PSS), carboxymethyl cellulose (CMC), and polyaspartate (PAP). The stability time of the freshly prepared RNIP modified by PSS and PAP in solution was around 7 and 20 min, respectively; while the stability time of bare RNIP was around 5 min, in this case. They suggested that particle stability depends on the adsorbed layer thickness of each modifier. This adsorbed layer would provide a barrier that prevents rapid particle agglomeration, avoiding the formation of large iron particle aggregates. Green polymers such as guar gum, potato starch, and alginate have been also added to RNIP suspensions to improve RNIP stability (Tiraferrri et al., 2008; Tiraferrri and Sethi, 2009). Visual tests indicated that guar gum yielded the most stable RNIP suspensions compared to potato starch and alginate.

Fewer studies have focused on pre-synthesis addition of stabilizers to limit nZVI aggregation. When the stabilizer is included as a component of the nZVI precursor solution (i.e., before reduction of the precursor ionic iron) stable aqueous nZVI suspensions have been successfully synthesized. For instance, Schrick et al. (2004) used hydrophilic carbon and poly (acrylic acid) (PAA) during nZVI synthesis. The stability of these modified-nZVI suspensions improved dramatically when com-

pared to bare nZVI suspensions. The suspension stability in turn helped to improve mobility through sand and clay-rich soil. In their study almost 100% and 60% of the modified particles were eluted from the sand and clay-rich soil packed columns, respectively; while only ~10% and ~20% of unmodified iron nanoparticles were eluted from slit-/sand-rich soil and clay-rich soil packed columns, respectively. In another study, He and Zhao (2005, 2007) and He et al. (2007) synthesized nZVI in the presence of a food-grade starch and CMC. This approach significantly improved nZVI stability. With visual observations suggesting that nZVI remained in suspension on the order of days with these stabilizers whereas it only remained in suspension on the order of minutes for bare nZVI. They hypothesized that improved nZVI stability was due to complexation of the Fe precursor ions with the carboxylate and hydroxyl groups present in CMC and starch, respectively. Complexation of these ions during the reduction process would not only prevent nucleation of large size nanoparticles but also lead to a material in which the CMC/starch molecules are strongly attached to the iron nanoparticle surface, preventing particle agglomeration. Furthermore, they also studied the effect of CMC molecular weight and degree of substitution (the density of COO⁻ groups present in CMC) and found that CMC with greater molecular weight and higher COO⁻ density produced smaller nanoparticles.

The results described above indicate that both electrostatic and steric hindrances are very important in the stabilization of nZVI in aqueous solutions. Clearly, the molecular structure of the stabilizers used, (e.g., formal or partial electrostatic charge in the anionic polyelectrolyte, functional group as indicated by the carboxylate/hydroxyl group results presented for CMC and starch, and size (i.e., molecular weight)) impacts its ability to suspend iron nanoparticles in aqueous solutions. Moreover, pre-synthesis addition of stabilizers appears to yield nZVI suspensions with enhanced stability when compared to post-synthesis addition of stabilizers (He and Zhao, 2007).

Although particle stability is very important for effective delivery of nZVI to contaminated source zones it is also important that these stabilized nZVI particles are able to rapidly degrade the target contaminant. He et al. (2007) found that the pre-synthesis addition of CMC to a Fe nanoparticle precursor solution lead to TCE degradation rates that were 17 times faster when compared to degradation with bare nZVI. Increased reaction rates have been attributed to reduced nZVI particle size in the pre-synthesis approach, leading to a larger surface area to weight ratio. On the other hand, post-synthesis stabilization of commercially available RNIP, using a triblock copolymer, surfactants, and anionic polyelectrolytes (PSS, PAP, and CMC) lead to reduced reactivity when compared to bare RNIP (Saleh et al., 2007). The decrease in reaction rates was a function of the stabilizer used and concentration of the stabilizer (Phenrat et al., 2009; Saleh et al., 2007). The authors suggested that decreased reactivity was due to the adsorbed modifiers inhibiting diffusion of TCE molecules to nZVI surface active sites (i.e., site blocking). A review of the literature suggests that synthesizing nZVI in the presence of stabilizers (pre-synthesis) yields more reactive nZVI particles when compared to adding stabilizers to commercially available Fe nanoparticles (post-synthesis).

In this contribution, bimetallic iron palladium (FePd) nanoparticles are synthesized using polyvinylpyrrolidone (PVP), carboxymethyl cellulose (CMC), and guar gum using a pre-synthesis addition approach to compare the stability and reactivity of these modified FePd nanoparticles. Even though guar gum was used in previous studies, to the best of our knowledge this is the first time that it has been used as a pre-synthesis stabilizer. PVP has been successfully used in the past to stabilize Pd nanoparticles in aqueous suspensions (Teranishi and Miyake, 1998) and has also improved the stability of iron based magnetorheological fluids prepared with iron powder (4.6 μm) (Hong Ting et al., 2006), but to the best of our knowledge, this is the first time it has been used for nZVI synthesis. Although CMC stabilizers have been studied extensively (He and Zhao, 2007; He and Zhao, 2008; He et al., 2007) this contribution presents a systematic comparison of both nZVI suspension stability and dechlorination reactivity for CMC, PVP and guar gum under similar conditions. The results presented herein will enable researchers to further explore mechanisms for nZVI stabilization as well as provide important considerations for the design of successful nZVI/stabilizer formulations for field applications.

2. Materials and method

2.1. Chemicals

Ferrous sulphate heptahydrate ($\text{FeSO}_4 \cdot 7\text{H}_2\text{O}$, Acros Organics), sodium borohydride (NaBH_4 , Sigma Aldrich), sodium carboxymethyl cellulose (CMC, MW = 90,000 and 250,000, Acros Organics, MW = 700,000 received from Sigma Aldrich), potassium hexachloropalladate (IV) (K_2PdCl_6 , Acros Organics), trichloroethylene (TCE, 99.5%, BDH), and hexane (environmental grade, Acros Organics) were used as received.

2.2. Nanoparticles preparation

FePd nanoparticles were prepared using a water-based approach (He et al., 2007) in an anaerobic chamber. All water was deionized using a Barnstead Easypure II system. Water and stabilizer solution were deoxygenated with N_2 gas prior to use. Freshly prepared $\text{FeSO}_4 \cdot 7\text{H}_2\text{O}$ solution and stabilizer solution were shaken for 5 min. Fe^{2+} ions were then reduced by adding NaBH_4 solution ($\text{BH}_4^-/\text{Fe}^{2+}$ molar ratio of 2) drop wise. Following the addition of NaBH_4 the suspension was continually shaken for 15 min before adding K_2PdCl_6 solution to the Fe-stabilizer suspension. The Pd loading in this study was 0.1 wt.% of Fe.

2.3. Physical characterization

The freshly synthesized FePd suspension and bare FePd nanoparticles were characterized for dispersion stability by visual inspection of settling behaviour (taking pictures at specific times to monitor the settling process) and also quantitatively by measuring the sedimentation rate of nanoparticles suspensions using a UV–vis spectrophotometer. To perform the first series of experiments, after FePd synthesis, part of the nanoparticle suspension was transferred into 10 mL serum bottle and capped with a Mininert® Valve to prevent air oxidation during the stability test. The stability of the nanoparticle suspension was evaluated by taking photographs of undisturbed FePd nanopar-

ticle suspensions every hour for two days. The pictures for each FePd nanoparticle formulation were then compared. For the second set of experiments a UV–vis spectrophotometer was used to measure the optical density at $\lambda = 500$ nm of the undiluted and undisturbed suspension. The absorbance values obtained at this wavelength were used to obtain a sedimentation curve. Freshly synthesized nZVI suspensions were transferred into the spectrophotometer cell using a screw cap photometric cell to prevent air oxidation. The optical density of the nanoparticles suspension was measured every 30 s for 48 h. Stability time is defined as the time required to achieve an absorbance value that is 50% of the initial value ($I/I_0 = 0.5$).

TEM analysis was performed using a Philips CM 10 and a FEI Titan 80–300 Cryo-in-situ Transmission Electron Microscope. The samples were prepared under anaerobic conditions by dropping 1 drop of freshly synthesized nanoparticles on a lacey carbon copper grid. The samples were then dried in a desiccator under a vacuum. A representative set of micrographs were obtained on each sample, and the diameter of each particle on those micrographs was measured in order to obtain diameter distributions. For samples analyzed using the Philips CM 10 TEM, nanoparticle diameter were measured using a CCD based camera system software (Advanced Microscopy Techniques Corp., Version 5 rev. 3). The particle size of the non-stabilized nanoparticles was determined using the iron oxide layer that surrounds each of nanoparticle as indication of the boundary between each particle. When samples were analyzed with the FEI Titan 80–300 TEM, the nanoparticle diameter was measured using Adobe Photoshop® 7.0 software. Electrophoretic mobility of the stabilizer solution (i.e., in the absence of nZVI) was measured using a Zeta Potential Analyzer (Model: Zeta Plus, Brookhaven Instruments Corporation, New York). For electrophoretic mobility experiments, a blank stabilizer solution was prepared by dissolving the desired amount of stabilizer in ultrapure water (Barnstead Easypure II system) and transferred into 4.5 mL optical polystyrene cuvettes with 4 optical windows for analysis. The pH of the resulting solution was also measured using ORION 5-Star Multiparameter meter (Thermo Electron). Viscosity measurements were carried out using a Brookfield DV-III Ultra rheometer.

2.4. TCE dechlorination

Batch reactivity experiments were conducted in 60 mL serum bottles. 55 mL of synthesized FePd nanoparticle suspension was added to the bottles and capped with a Teflon mininert valve. 50 μL of TCE stock solution was then added to the bottle to obtain an initial TCE concentration of 50 mg/L. The bottle was then shaken using a wrist-action shaker. 0.25 mL of this suspension was sampled at selected times and transferred to a 2 mL GC vial containing 1 mL of hexane for TCE extraction. The extraction was then analyzed using an Agilent 7890A GC equipped with an electron capture detector (ECD) and a DB-624 (30 m \times 0.53 mm, 3.0 μm) column.

3. Results and discussion

3.1. TEM and diameter distribution

TEM micrographs for nonstabilized and stabilized FePd nanoparticles, using the pre-synthesis approach, are shown in

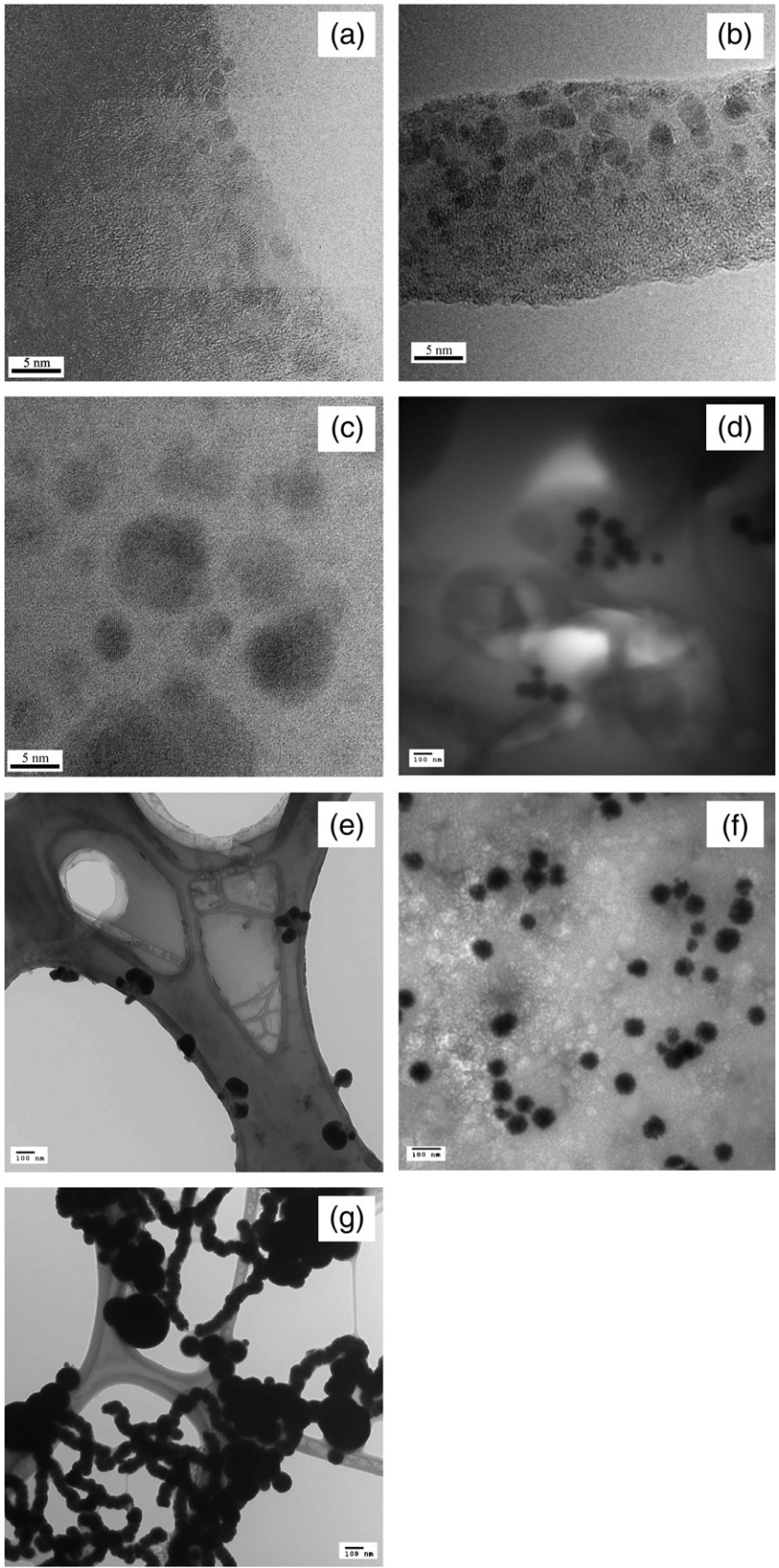


Fig. 1. The stabilized FePd nanoparticles were assessed at three different molecular weights (90 K, 250 K, and 700 K) of 0.2% carboxymethyl cellulose (CMC), two different molecular weights (40 K and 360 K) of 1% polyvinylpyrrolidone (PVP) as well as 0.05% guar gum. TEM micrographs at 0.1% guar gum were not obtained, however stability experiments were conducted at this concentration and will be discussed later. The diameter distributions obtained for each sample are shown in Fig. 2. The micrographs obtained for the particles synthesized using CMC 700 K and 250 K indicate that the particles were well dispersed (i.e., each particle is distinct and isolated). Moreover they were both (700 K and 250 K) similar in size (mean particle diameters were 2.4 and 2.8 nm, respectively) and had a narrow particle size distribution. For the case of CMC90K, the particles were larger and had a broader particle size distribution than those obtained using higher molecular weight CMC (mean diameter of 18.8 nm). On the other hand FePd particles synthesized using PVP360K, PVP40K and guar gum were larger, with mean particles diameters of 87.3, 74.5, and 63.1 nm, respectively. All of these stabilized FePd nanoparticles (PVP, CMC, guar gum) had a smaller mean diameter than the nonstabilized FePd nanoparticles, which had a mean diameter of 100.7 nm.

The molecular structure, pH, and electrophoretic mobility of each stabilizer are shown in Table 1. The electrophoretic mobility for CMC indicates a net negative surface charge that is independent of molecular weight. Previous studies on the effect of molecular weight of polystyrene sulfonate on its electrophoretic mobility showed that for a polymer with a degree of polymerization above 20, the electrophoretic mobility remains nearly constant (Böhme and Scheler, 2007). This is consistent with the results shown on Table 1. The electrophoretic mobility values obtained for PVP and guar gum stabilizers indicate that they are neutral. The functional groups present on each of these stabilizers differ, leading to differences in measured electrophoretic mobility. In the case of the CMC molecule carboxylate ($-\text{COO}^-$) and hydroxyl ($-\text{OH}$) functional groups are present. However in the case of guar gum only the hydroxyl functional group is present. Finally the PVP molecule has a carbonyl group (CO) which bears two lone pairs of electrons at the oxygen atom. Differences in the measured nanoparticle size (Fig. 2) can be explained by the differing molecular structure of these stabilizers. For example He and Zhao (2007) investigated the stability of iron nanoparticles suspensions synthesized in the presence of CMC. They proposed that the carboxylate group present in the CMC strongly complexes the Fe^{2+} ions in solution (i.e., precursor to nZVI particles), thereby dispersing Fe^{2+} ions throughout the CMC network, which are then rapidly nucleated after borohydride reduction. He and Zhao (2007) suggested that as the iron nanoparticles grow to a critical size their growth is limited due to steric and electrostatic hindrances caused by the attachment of CMC molecules at the particle surface. Results from this present study indicate that with increased CMC molecular weight (from 90 K to 700 K) the average particle size (as observed by TEM) decreased from 18.8 nm to 2.4 nm. This is in agreement with increased steric hindrance that results when CMC molecules

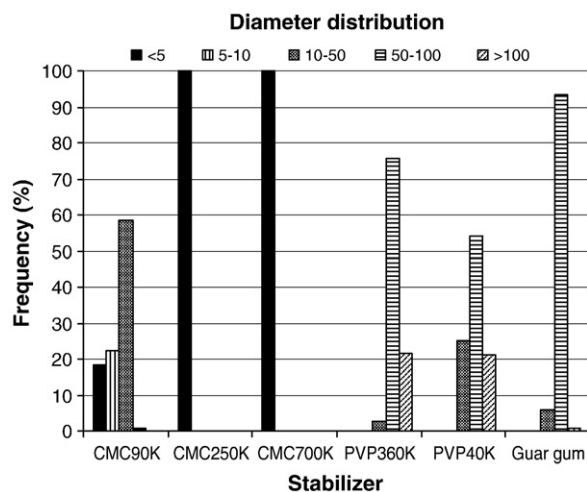
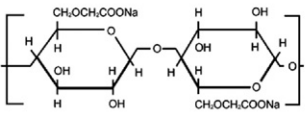
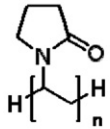
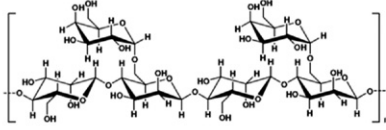


Fig. 2. Diameter distributions of nonstabilized and stabilized FePd nanoparticles from TEM images. The particles count are 103, 43, 25, 74, 101, 134, and 132 particles for CMC 90K, CMC250K, CMC700K, PVP360K, PVP40K, Guar gum (0.05%), and nonstabilized FePd, respectively.

with higher molecular weight are used during synthesis. Electrostatic interactions are also important. CMC, with a net negative charge, limits nanoparticle growth in comparison to the other neutrally charged stabilizers (i.e., PVP and guar gum) whose use resulted in larger nanoparticles. In the case of PVP there are two important differences when compared to CMC. The first is that Fe^{2+} ions likely form weak bonds with the lone pair electrons at the oxygen atom on the PVP carbonyl group. The interaction between PVP and Fe^{2+} (i.e., lone pair electrons and Fe^{2+}) is weaker than $\text{CMC}-\text{Fe}^{2+}$ interactions (i.e., $\text{Fe}^{2+}/-\text{COO}^-$) since the carboxylate group bears a formal negative charge compared to the lone pair electron at the oxygen atom on the PVP carbonyl group. As the $\text{PVP}-\text{Fe}^{2+}$ interaction is not as strong as $\text{CMC}-\text{Fe}^{2+}$, this results in slower Fe cluster nucleation when sodium borohydride was introduced. Generally, slow cluster nucleation leads to the formation of larger particles as there is sufficient time for cluster agglomeration during the process. The second important difference is that the PVP is neutral compared to CMC. This results in weaker electrostatic interactions between Fe and PVP. As such it is a predominantly steric hindrance that prevents further nanoparticle growth, which is not as effective as when both steric and electrostatic interactions limit particle size, as is the case with CMC stabilizers. This would explain the larger particle size obtained using PVP as a stabilizer. This explanation could also be used to explain particle size differences observed when guar gum and CMC are used as stabilizers. The guar gum/ Fe^{2+} interactions would also be weaker than $\text{CMC}-\text{Fe}^{2+}$ interactions as there is only one lone electron pair from the oxygen atom in the hydroxyl group which could form a bond with Fe^{2+} . Therefore, this would result in slower Fe cluster nucleation as in the case of PVP. Although both PVP and guar gum result in slow Fe cluster nucleation, as they lack a formal charge, their Fe^{2+} complexation capacity differ. In the case of guar gum, hydroxyl groups

Table 1

Molecular structure, pH, and electrophoretic mobility of (a) CMC, (b) PVP, and (c) guar gum solution.

Stabilizers	Structure	Molecular weight (g/mol)	pH*	Electrophoretic mobility*
CMC		700K	7.1	-5.9
		250K	7.0	-4.6
		90K	7.0	-5.0
PVP		360K	5.5	0.03
		40K	4.4	-0.99
Guar gum			6.6	-0.05

*pH and electrophoretic mobility of stabilizer solution measured at the same concentration used to synthesize FePd nanoparticles suspension: 0.2%CMC, 1%PVP, and 0.05% guar gum.

are the ligands complexing the Fe^{2+} ions, while for PVP/ Fe^{2+} complexation occurs through carbonyl groups. The lone pairs present in the hydroxyl group have 25% of s character (sp^3) as opposed to the lone pairs in the carbonyl group present in PVP which have 33% s character (sp^2). It is well known that a decrease in s character in a lone pair leads to more effective complexation and stronger metal–ligand bonds. The hydroxyl group would therefore form more stable complexes with iron than a carbonyl group leading to observed differences in size when Fe nanoparticles were prepared using guar (hydroxyl groups complexing iron ions) as opposed to PVP (carbonyl groups complexing iron ions). Both PVP and guar gum are neutral compounds; consequently both stabilizers would only provide steric hindrance to counteract particle agglomeration (King, 2005). These mechanisms explain observed trends in size for the CMC, guar gum and PVP stabilized FePd nanoparticles.

3.2. Stability tests

The stability of FePd nanoparticles is shown in Fig. 3. Fe–Pd nanoparticles synthesized in the absence of a stabilizer settled rapidly (i.e., within 1 h) (Fig. 3f). Both the CMC and guar gum yielded stable FePd nanoparticle suspensions in excess of 48 h (Fig. 3a, d, and e) whereas PVP did not result in stable nanoparticle suspensions for an extended period (Fig. 3b and c). Furthermore the lower molecular weight PVP (PVP40K) yielded no improvement in FePd nanoparticle stability in comparison to bare FePd nanoparticles. The poor stability of PVP suspensions was somewhat surprising given that the amount of PVP used in the suspension (1 wt.%) was higher than that of CMC (0.2 wt.%) and guar gum (0.05 wt.%). Inspection of these photos suggests limited iron oxidation in the case of PVP 360 K and no oxidation in the other cases. Sedimentation curves (Fig. 4) are in good agreement with visual observations (Fig. 3). Guar gum yields the most stable suspension with a stability time of 48 h (i.e., time required to

achieve an absorption intensity that is 50% of the initial intensity ($I/I_0 = 0.5$)). Nanoparticles stabilized with the three different molecular weight CMCs yielded similar sedimentation curves, with stability times of 40 h. Nanoparticles stabilized with PVP360K were less stable than CMC (stability time of 9 h) however PVP360K performed much better than PVP40K and bare nanoparticles which settled out of solution in one hour. Field application of nanometals for remediation purposes would typically require that nanometals remain in suspension for extended periods of time so they can be delivered from an injection well to the contaminated source zone.

Improved stability of these nanoparticle suspensions is achieved through electrostatic repulsion and/or steric hindrance forces provided by the stabilizers. As discussed previously each stabilizer has differing molecular structure and electrophoretic mobility. The contribution of these repulsive interactions, when stabilizers are added pre-synthesis, will be discussed here in more detail. Higher molecular weight CMC stabilizers have resulted in smaller nanoparticles and faster TCE dechlorination reaction rates (He and Zhao, 2007, 2008) however the impact of CMC molecular weight on nanoparticle stability has not been reported. As shown in Fig. 4, increased CMC molecular weight did not improve nZVI stability as all CMC types exhibited similar sedimentation behaviour (Fig. 4). Increased CMC molecular weight should increase steric hindrance as polymer chain length increases, resulting in greater repulsive forces between particles. These results indicate that steric hindrance does not play a critical role in stabilizing FePd nanoparticles under these CMC solution conditions, even though steric hindrance played an important role in creating very small nanoparticles. It should be noted that increased CMC molecular weight does not decrease CMC charge as illustrated by the electrophoretic mobility. As the net charge of CMC is similar for each molecular weight and nanoparticle stability was similar for each molecular weight, enhanced FePd nanoparticle stability in CMC

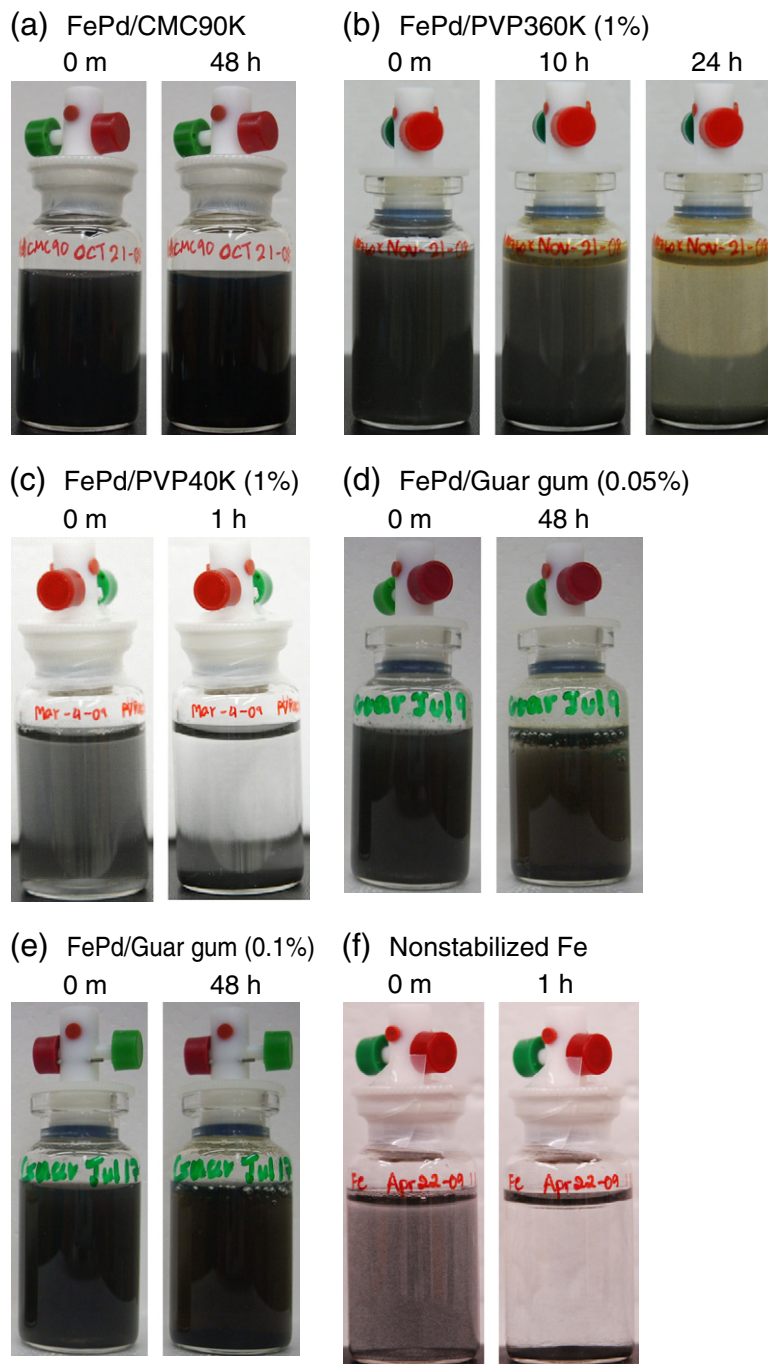


Fig. 3. Pictures of stabilized FePd nanoparticles using different polymer at various time. Fe loading is 0.1 g/L with Pd 0.1 wt.% of Fe; (a) CMC90K 0.2%, (b) PVP360K 1%, (c) PVP40K 1%, (d) guar gum 0.05%, (e) guar gum 0.1%, and (f) nonstabilized FePd.

suspensions mainly resulted from electrostatic interactions. It is also important to point out that nanoparticles synthesized in the presence of CMC were extremely small making them easier to stabilize when compared to larger nanoparticles. Magnetic attractive forces increase with r^6 (r = particle radius) (Phenrat et al., 2008) as such smaller particles would have significantly less magnetic attraction forces when compared to the larger particles synthesized in this study.

As discussed previously PVP40K did not improve nZVI stability (settling is observed within 1 h) but the higher molecular weight PVP stabilizer molecular weight significantly improved suspension stability. This behaviour is distinctly different than the behaviour observed for the CMC stabilizer, where an increase in CMC molecular weight did not improve suspension stability. As discussed above, the interaction between PVP and Fe^{2+} is weaker than CMC-Fe^{2+}

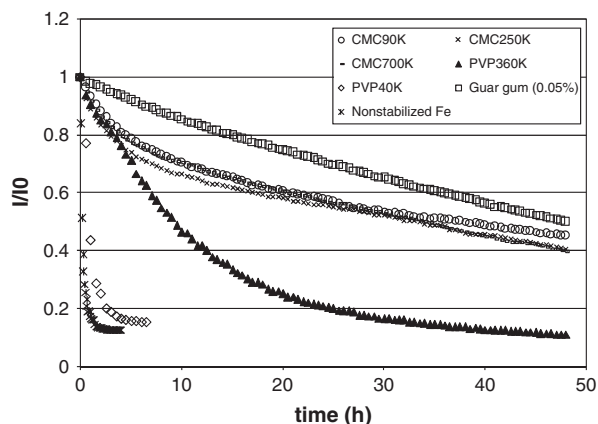


Fig. 4. Sedimentation curve of stabilized FePd at 0.1 g/L iron loading Pd at 0.1 wt.% of Fe.

interactions since the carboxylate group in CMC bears a formal negative charge compared to the lone pair electrons of the CO group in PVP. Given this weaker complexation prior to reduction Fe nanoparticles would not be strongly attached to the PVP molecule when compared to Fe nanoparticles synthesized in CMC solution. Since Fe nanoparticles are not strongly attached to PVP, Fe nanoparticles could more easily sinter and agglomerate. This would explain the better suspension stability obtained from CMC compared to PVP. PVP is a neutral molecule as such FePd nanoparticle stabilization enhancement would be mainly due to steric hindrance. Improved FePd nanoparticle stability with increased PVP molecular weight is expected as the longer polymer chain (i.e., PVP360K) adsorbed to the nanoparticle surface provides greater steric hindrance between nanoparticles. As discussed above FePd nanoparticles synthesized in the presence of CMC were much smaller and more stable than those synthesized with PVP. The ratio of magnetic forces between FePd nanoparticles synthesized using PVP, assuming a representative particle size of 70 nm, to those synthesized using CMC, assuming a representative particle size of 3 nm, is 10^8 . This significant difference in attractive forces could have contributed to the poor stability of the PVP stabilized FePd nanoparticles as PVP stabilizers would have to impart significantly more repulsive forces in comparison to CMC.

The best stabilization results were obtained using guar gum, a relative large macromolecule. This dramatic improvement in FePd nanoparticle stability is interesting as guar gum is neutral eliminating the potential for electrostatic hindrance, leaving steric hindrance as a possible stabilization mechanism. Tiraferri et al. (2008) also observed improved suspension stability using commercially available iron nanoparticles (RNIP) and guar gum (post-synthesis addition of stabilizer). They reported that at 1.5 g/L RNIP and 0.4% guar, the nanoparticles only remained suspended for a few hours, considerably less than that observed here (stability time of 48 h). However the ratio of guar gum weight to iron nanoparticle weight was higher in this study in comparison to their study (i.e., 2.67 in their study; 5 and 10 in this study). Given that guar gum did not dramatically improve RNIP stability, as observed in this study, this suggests that mechanisms in addition to steric hindrance improved the stability of the FePd nanoparticles. In this study, the nanopar-

ticles were synthesized using borohydride as a reducing agent resulting in the formation of borate ions ($B(OH)_4^-$) as a by-product. Borate can act as a cross-linker of polymer chains in certain polyols, such as PVA and guar gum, leading to spontaneous gel formation (Peter, 2007). In this study the viscosity of the guar solution increased following borohydride addition during nZVI synthesis (i.e., viscosity increased from 2.2 cp to 6.0 cp). The formation of this guar gel and subsequent increases in suspension viscosity further improves nanometal stability by slowing down nanoparticle Brownian motion that leads to agglomeration. The formation of the guar gel will be further discussed in the context of observed TCE dechlorination results in the next section.

In summary for the case of CMC the formation of a stabilizer- Fe^{2+} coordination complex and electrostatic interactions, rather than steric hindrance, seem to be the most important mechanisms enhancing FePd nanoparticle stability. Increasing the molecular weight of the CMC molecule did not impact the stability of the CMC/nanoparticle suspension. For the case of PVP, where a weaker coordination bond is formed between the iron ion precursor and the stabilizer, steric hindrance was the main nanoparticle stabilization mechanism. With guar gum, gelation of the guar solution, with borate ions, and subsequent increases in suspension viscosity, enhanced FePd nanoparticle suspension stability. With gelation nanoparticles are entrapped inside the guar gel matrix, preventing particle agglomeration. In this case, the molecular structure of guar gel is very large compared to CMC and PVP.

3.3. TCE dechlorination

The impact of the physical properties (e.g., surface area) of nonstabilized and stabilized FePd nanoparticles on reactivity was evaluated by measuring TCE dechlorination reaction rates. The stabilized FePd nanoparticles exhibited higher reactivity when compared to the nonstabilized material, with the exception of nanoparticles stabilized with PVP40K and guar gum (Fig. 5). For example both FePd/CMC700 K and FePd/CMC250K completely degraded TCE within 6 h, FePd/CMC90K and PVP360K degraded the 50 mg/L of TCE within 24 h but nonstabilized FePd only removed 37% of the TCE within 24 h. Pseudo-first order relationships fit to observed degradation data suggests that FePd/CMC90K degrades TCE faster than FePd/PVP360K (Table 2). When FePd/guar gum 0.05% was used about 50% of the TCE remained after 24 h. However, when the guar gum stabilizing concentration was increased to 0.1%, less than 10% of initial the TCE was reduced after 24 h.

The highest reactivity was observed when CMC (90 K, 250 K, and 700 K) was used as a stabilizer. Degradation of chlorinated compounds via nZVI is a surface mediated reaction that occurs on the surface of the Fe nanoparticles. A smaller average particle size distribution yields a higher surface area per mass of nanoparticle. The higher reactivity observed for CMC stabilized nanoparticles is attributed to the very small diameter, and large surface area, associated with these nanoparticles (i.e., the mean particle diameters were 18.8, 2.8, and 2.4 nm for CMC90K, 250 K, and 700 K, respectively). Pseudo-first order rate constants (k_{obs} , h^{-1}), fit to observed degradation data, indicate the following order of reactivity, FePd stabilized with CMC 250 K and

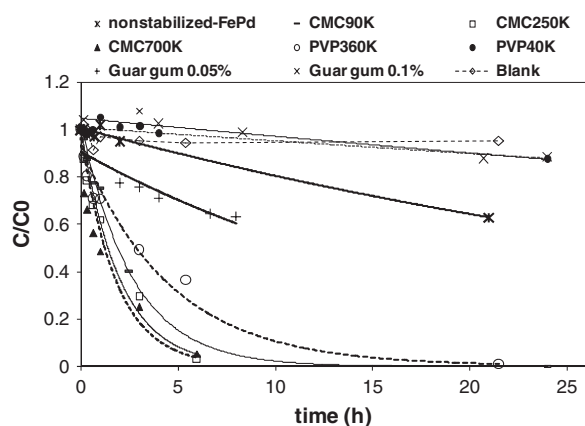


Fig. 5. TCE dechlorination using nonstabilized and stabilized FePd nanoparticles suspension. Initial TCE concentration (C_0) = 50 mg/L, iron loading = 0.1 g/L, Pd loading = 0.1 wt.% of Fe.

700 K > CMC90K > PVP360K > guar gum (0.05%) > nonstabilized FePd > guar gum (0.1%) ~ PVP40K. When PVP360K and guar gum were used to stabilize FePd the particles were smaller than nonstabilized FePd particles but larger than those obtained using CMC, consistent with the reactivity trend. FePd particles stabilized with PVP360K, PVP40K and guar gum (0.05%) all had a similar range of particle diameters (i.e., differences of 30%) however reactivity varied by a factor of 33 (Table 2). PVP40K stabilized FePd nanoparticles yielded the lowest pseudo-first order rate constant, likely due to its very poor stability and strong tendency to aggregate in aqueous suspensions, thus limiting available surface sites for TCE degradation. FePd synthesized in the presence of guar gum also resulted in slow TCE degradation. As discussed previously, the FePd nanoparticles were synthesized using borohydride as a reductant resulting in gelation of the guar gum in the presence of borate ($B(OH)_4^-$) ions during synthesis. When gelation occurs, a three-dimensional macromolecular structure is formed, trapping the FePd particles, limiting accessibility of reactive nanoparticle sites. Moreover this might also inhibit the mass transfer of TCE from the aqueous phase to the reactive sites. The hypothesis of site inaccessibility was further confirmed when increased guar gum concentration (i.e., from 0.05% to 0.1%) further decreased the TCE dechlorination rate. Increasing guar gum concentrations would result in gelation that forms systems of larger molecular structures, trapping larger amounts of FePd

particles, resulting in further reduction of TCE dechlorination reactivity.

Phenrat et al. (2009) recently reported the effects of adsorbed polyelectrolytes on the dechlorination of TCE via Fe nanoparticles. They found that an adsorbed polyelectrolyte can decrease Fe dechlorination activity by either blocking reactive surface sites (at low surface excess) when polymer adsorption is such that the length of the polymer is in contact with the nanoparticle surface or by a combination of site blocking and decrease in aqueous TCE concentrations near the nZVI surface (at high surface excess). He and Zhao (2008) have also found that when the CMC90K–Fe molar ratio increased from 0.0124 to 0.061, the rate of dechlorination declined. They suggested that adsorbed CMC molecules form a more compact surface coating at higher CMC–Fe molar ratios, blocking available Fe reactive sites and inhibiting mass transfer of TCE from the bulk solution to the nanoparticle surface. These effects could be used to explain FePd/PVP40K results. The PVP40K–Fe molar ratio used in this study is 0.139, which was relatively high compared to the CMC90K–Fe ratio used in the He and Zhao work. As such it is possible that the PVP40K molecules adsorbed densely on the nZVI surface, resulting in the blockage of active sites. In the case of PVP360K, the PVP360K–Fe molar ratio is 0.0155, which is only slightly higher than the molar ratio used in the CMC90K system (0.0124). He and Zhao (2008) observed that increasing the CMC90K–Fe molar ratio from 0.0124 to 0.0186, had a very limited impact on observed rate constants. Given that the amount of PVP used is similar to CMC site blocking by PVP360K does not likely play an important role in differences in observed rate constants between PVP360K and CMC90K in this study. It is more likely that the difference in observed rate constants is due to differences in particle size. However, a more detailed investigation is needed to clarify the effect of PVP40K on TCE dechlorination reactivity.

As mentioned above, a pseudo-first order reaction model (Eq. (1)) was used to fit the reactivity data

$$-\frac{dC}{dt} = k_{obs}C = k_{SA}a_s\rho_m C \quad (1)$$

where C is the TCE concentration (mg/L) at time t (h), k_{obs} is the observed rate constant (h^{-1}), k_{SA} is the surface area-based rate constant ($L h^{-1} m^{-2}$), a_s is the TEM based specific surface area of the nanoparticles ($m^2 g^{-1}$), and ρ_m is the mass concentration of the nanoparticles (g/L). Surface area-normalized rate constants (k_{SA} , $L h^{-1} m^{-2}$) were calculated

Table 2

Mean diameter of stabilized and nonstabilized FePd nanoparticles obtained from TEM analysis. Surface area was calculated from surface area = $3 \times 10^6 / (r \times \rho)$; r = particle radius (nm), ρ = density of Fe = 7870 kg/m³ (He and Zhao, 2005).

Stabilizers	$k_{obs}(h^{-1})$	Mean diameter (nm), TEM	Surface area (m^2/g), calculated from TEM mean diameter	k_{SA} ($L/h/m^2$)
CMC90K	0.381	18.8	41	0.093
CMC250K	0.557	2.8	269	0.021
CMC700K	0.497	2.4	317	0.016
PVP360K	0.219	87.3	8.73	0.251
PVP40K	0.006	74.5	10.23	0.006
Guar gum (0.05%)	0.051	63.1	12.08	0.042
Guar gum (0.1%)	0.0075	–	–	–
nonstabilized	0.022	100.7	7.57	0.029

based on the mean particle radius obtained from the TEM micrographs suggest that dechlorination trends based on observed rate constants (k_{obs}) may not properly reflect dechlorination activity (Table 2). FePd/PVP360K exhibits the largest k_{SA} ($k_{SA} = 0.251 \text{ L h}^{-1} \text{ m}^{-2}$) followed by FePd/CMC90K, FePd/guar gum (0.05%), nonstabilized FePd, FePd/CMC250K, FePd/CMC700K and then FePd/PVP40K. He and Zhao (2008) reported a k_{SA} value of $0.0064 \text{ L h}^{-1} \text{ m}^2$ based on TEM-calculated surface area for FePd/CMC90K (Fe loading 0.1 g/L, Pd 0.1% of Fe, CMC 0.2%, and initial TCE = 20 mg/L). The surface area-normalized rate constants are higher in this study with the exception of the FePd/PVP40K and FePd/guar gum (0.1%) systems. It should be noted, however, that they purged their reaction bottle with N_2 before adding TCE to the system, removing any residual H_2 that was produced during synthesis. This may be the reason for the observed differences in the k_{SA} value.

It is important to point out that these reactivity experiments were carried out under ideal conditions (i.e., ultrapure water, synthesis and reactivity experiments under anaerobic conditions). These ideal conditions would be difficult to replicate in the field. For example small amounts of oxygen may be present in the field during synthesis, injection or in the aquifer. In these cases a stabilizer similar to FePd/PVP360K might be a better candidate than FePd/CMC for site remediation as the smaller particles are more easily oxidized, resulting in reduced capacity to degrade the target contaminants. Furthermore, dissolved groundwater solutes such as NO_3^- , Cl^- , HCO_3^- , SO_4^{2-} , and HPO_4^{2-} can negatively impact iron nanoparticle reactivity (Liu et al., 2007) and stability. In this case FePd/guar gum may be an appropriate choice even though it is not as reactive as FePd/CMC or FePd/PVP360K. The nanoparticles are encapsulated during the guar gum gelation process and would be slowly released with time. As such they are less susceptible to side reactions that lower FePd remediation capacity prior to reaching the contaminated source zone. In summary site conditions and the particular application should be carefully considered prior to selection of a suitable stabilized nanometal suspension. The optimal selection may not be the nanometal with the highest reactivity.

4. Conclusions

The stabilizers used in this study provide some important insights related to FePd stabilization mechanisms. Sodium carboxymethyl cellulose (CMC) and guar gum yielded more stable nanoparticle suspensions when compared to polyvinylpyrrolidone (PVP). The difference in stabilizer performance is due to differing stabilizer molecular structure and stabilization mechanisms. The main mechanism in CMC mediated stability is electrostatic interaction while for PVP steric hindrance is the main stabilizing mechanism. For guar gum, cross-linking by borate ions increased suspension viscosity yielding outstanding nanoparticle stability. With regards to reactivity TCE degradation was fastest for FePd/CMC followed by FePd/PVP360K. Surface area-based rate constants, however, exhibited a different trend, with FePd/PVP360K yielding the largest k_{SA} . Overall, CMC yielded FePd nanoparticles with enhanced suspension stability and reactivity. However, their particle size makes them susceptible to oxidation when compared to larger particles obtaining using other stabilizers.

The results reported in this contribution indicate that a successful stabilizer must offer a mechanism for stability that does not affect reactivity. Moreover, complexation of iron precursors during synthesis plays a key role in nZVI stabilization. Thus a polymer that has functional groups able to complex iron ions would most likely be a successful candidate for nZVI stabilization, as long as this bond or associated steric hindrance does not affect accessibility of the chlorinated hydrocarbon to reaction sites. The stabilizers that fit this category include a wide family of materials that need to be further explored.

References

- Böhme, U., Scheler, U., 2007. Hydrodynamic size and electrophoretic mobility of poly(styrene sulfonate) versus molecular weight. *Macromol. Chem. Phys.* 208 (19–20), 2254–2257.
- Cosgrove, T., 2005. *Colloid Science-Principles, Methods, and Applications*. Blackwell Publishing, Oxford.
- He, F., Zhao, D., 2005. Preparation and characterization of a new class of starch-stabilized bimetallic nanoparticles for degradation of chlorinated hydrocarbons in water. *Environ. Sci. Technol.* 39 (9), 3314–3320.
- He, F., Zhao, D., 2007. Manipulating the size and dispersibility of zerovalent iron nanoparticles by use of carboxymethyl cellulose stabilizers. *Environ. Sci. Technol.* 41 (17), 6216–6221.
- He, F., Zhao, D., 2008. Hydrodechlorination of trichloroethene using stabilized Fe–Pd nanoparticles: reaction mechanism and effects of stabilizers, catalysts and reaction conditions. *Appl. Catal. B* 84 (3–4), 533–540.
- He, F., Zhao, D., Liu, J., Roberts, C.B., 2007. Stabilization of Fe^{0} /Pd nanoparticles with sodium carboxymethyl cellulose for enhanced transport and dechlorination of trichloroethylene in soil and groundwater. *Ind. Eng. Chem. Res.* 46 (1), 29–34.
- Hong Ting, P., Feng Jing, J., Zhenglong, Y., Biao, Y., Xin, L., 2006. Effects of polyvinylpyrrolidone and carbon nanotubes on magnetorheological properties of iron-based magnetorheological fluids. *J. Appl. Polym. Sci.* 102 (2), 1653–1657.
- Kanel, S.R., Goswami, R.R., Clement, T.P., Barnett, M.O., Zhao, D., 2008. Two dimensional transport characteristics of surface stabilized zero-valent iron nanoparticles in porous media. *Environ. Sci. Technol.* 42 (3), 896–900.
- Kim, H.-J., Phenrat, T., Tilton, R.D., Lowry, G.V., 2009. Fe^{0} nanoparticles remain mobile in porous media after aging due to slow desorption of polymeric surface modifiers. *Environ. Sci. Technol.* 43 (10), 3824–3830.
- King, R.B., 2005. *Encyclopedia of Inorganic Chemistry*. In: King, R.B. (Ed.), John Wiley and Sons, Inc, NJ, p. 4154.
- Li, X.-q., Elliott, D.W., Zhang, W.-X., 2006. Zero-valent iron nanoparticles for abatement of environmental pollutants: materials and engineering aspects. *Crit. Rev. Solid State Mater. Sci.* 31 (4), 111–122.
- Lien, H.-L., Zhang, W.-x., 1999. Transformation of chlorinated methanes by nanoscale iron particles. *J. Environ. Eng.* 125 (11), 1042–1047.
- Lien, H.-L., Zhang, W.-x., 2001. Nanoscale iron particles for complete reduction of chlorinated ethenes. *Colloids Surf. A* 191 (1–2), 97–105.
- Liu, Y., Majetich, S.A., Tilton, R.D., Sholl, D.S., Lowry, G.V., 2005. TCE dechlorination rates, pathways, and efficiency of nanoscale iron particles with different properties. *Environ. Sci. Technol.* 39 (5), 1338–1345.
- Liu, Y., Phenrat, T., Lowry, G.V., 2007. Effect of TCE concentration and dissolved groundwater solutes on nZVI-promoted tce dechlorination and H_2 evolution. *Environ. Sci. Technol.* 41 (22), 7881–7887.
- Matheson, L.J., Tratnyek, P.G., 1994. Reductive dehalogenation of chlorinated methanes by iron metal. *Environ. Sci. Technol.* 28 (12), 2045–2053.
- Orth, W.S., Gillham, R.W., 1996. Dechlorination of trichloroethene in aqueous solution using Fe^0 . *Environ. Sci. Technol.* 30 (1), 66–71.
- Peter, A.W., 2007. Gelling agents. In: Peter, A.W. (Ed.), *Handbook of Industrial Water Soluble Polymers*, pp. 73–97.
- Phenrat, T., Saleh, N., Sirk, K., Tilton, R.D., Lowry, G.V., 2007. Aggregation and sedimentation of aqueous nanoscale zerovalent iron dispersions. *Environ. Sci. Technol.* 41 (1), 284–290.
- Phenrat, T., et al., 2008. Stabilization of aqueous nanoscale zerovalent iron dispersions by anionic polyelectrolytes: adsorbed anionic polyelectrolyte layer properties and their effect on aggregation and sedimentation. *J. Nanopart. Res.* 10 (5), 795–814.
- Phenrat, T., Liu, Y., Tilton, R.D., Lowry, G.V., 2009. Adsorbed polyelectrolyte coatings decrease Fe^0 nanoparticle reactivity with TCE in water: conceptual model and mechanisms. *Environ. Sci. Technol.* 43 (5), 1507–1514.
- Robert, W.G., Stephanie, F.O.H., 1994. Enhanced degradation of halogenated aliphatics by zero-valent iron. *Ground Water* 32 (6), 958–967.
- Saleh, N., et al., 2007. Surface modifications enhance nanoiron transport and nZVI targeting in saturated porous media. *Environ. Eng. Sci.* 24 (1), 45–57.

- Saleh, N., et al., 2008. Ionic strength and composition affect the mobility of surface-modified Fe⁰ nanoparticles in water-saturated sand columns. *Environ. Sci. Technol.* 42 (9), 3349–3355.
- Schrick, B., Hydutsky, B.W., Blough, J.L., Mallouk, T.E., 2004. Delivery vehicles for zerovalent metal nanoparticles in soil and groundwater. *Chem. Mater.* 16 (11), 2187–2193.
- Teranishi, T., Miyake, M., 1998. Size control of palladium nanoparticles and their crystal structures. *Chem. Mater.* 10 (2), 594–600.
- Tiraferrri, A., Sethi, R., 2009. Enhanced transport of zerovalent iron nanoparticles in saturated porous media by guar gum. *J. Nanopart. Res.* 11 (3), 635–645.
- Tiraferrri, A., Chen, K.L., Sethi, R., Elimelech, M., 2008. Reduced aggregation and sedimentation of zero-valent iron nanoparticles in the presence of guar gum. *J. Colloid Interface Sci.* 324 (1–2), 71–79.
- Wang, C.-B., Zhang, W.-x., 1997. Synthesizing nanoscale iron particles for rapid and complete dechlorination of TCE and PCBs. *Environ. Sci. Technol.* 31 (7), 2154–2156.
- Zhang, W.-X., Daniel, W.E., 2006. Applications of iron nanoparticles for groundwater remediation. *Remediation J.* 16 (2), 7–21.